On the generation of a helicopter aerodynamic database

M. Raffel
Markus.Raffel@dlr.de
German Aerospace Center (DLR), Goettingen, Germany

F. De Gregorio
Centro Italiano Ricerche Aerospaziali (CIRA), Capua, Italy

K. de Groot and O.Schneider
German Aerospace Center (DLR), Braunschweig, Germany

W. Sheng
Department of Aerospace Engineering, University of Glasgow, UK

G. Gibertini
Dipartimento di Ingegneria Aerospaziale, Politecnico di Milano, Italy

A. Seraudie
Aerodynamics and Energetics Model Department, ONERA, Toulouse, France

ABSTRACT

The GOAHEAD (Generation of an Advanced Helicopter Experimental Aerodynamic Database for CFD code validation) consortium was created in the frame of an EU-project in order to create an experimental database for the validation of 3D-CFD and comprehensive aeromechanics methods for the prediction of unsteady viscous flows. This included the rotor dynamics for complete helicopter configurations, i.e. main rotor – fuselage – tail rotor configurations with emphasis on viscous phenomena like flow separation and transition from laminar to turbulent flow. The wind tunnel experiments have been performed during two weeks in the DNW-LLF on a Mach-scaled model of a modern transport helicopter consisting of the main rotor, the fuselage, control surfaces and the tail rotor. For the sake of controlled boundary conditions for later CFD validation, a closed test section has been used. The measurement comprised global forces of the main rotor and the fuselage, steady and unsteady pressures, transition positions, stream lines, position of flow separation, velocity profiles at the test section inlet, velocity fields in the model wake, vortex trajectories and elastic deformations of the main and tail rotor blades.

NOMENCLATURE

a	speed of sound, ms^{-1}
c	blade chord, m
u'^2	root mean square of velocitiy longitudinal component
v'^2	root mean square of velocitiy spanwise component
w'^2	root mean square of velocitiy vertical component
M_{WT}	Mach number of wind-tunnel flow, $M_{WT} = V_{WT}/a$
M_{MR}	Mach number of blade tip in hover, main rotor, $M_{MR} = (\Omega R)_{MR}/a$
M_{TR}	Mach number of blade tip in hover, tail rotor, $M_{TR} = (\Omega R)_{TR}/a$
R	blade radius, m
α_S	rotor shaft angle-of-attack
α_{fus}	fuselage angle-of-attack
μ	advance ratio M_{WT}/M_{MR}
ψ_{MR}	main rotor azimuth angle (0° = reference blade above the fuselage)
Ω	rotor rotational frequency, rad/s

Paper No. 3565. Manuscript received 19 April 2010, revised version received 28 September 2010, accepted 7 October 2010.

https://doi.org/10.1017/S0001924000005492 Published online by Cambridge University Press

1.0 INTRODUCTION

During the past decade considerable progress has been made in developing aerodynamic prediction capabilities for isolated helicopter components. In the same period, the isolated main rotor downwash structure has mainly been investigated by means of optical methods in hover flight conditions[1-5]. Today, leading edge CFD software systems are available, and others are being developed, which are capable of predicting the viscous flow around main rotor-fuselage configurations or even complete helicopters. The greatest shortcoming for qualifying these methods as design tools in the industrial design process is the lack of detailed experimental validation data for the aerodynamics of complete helicopters. To overcome this shortcoming, the GOAHEAD-consortium (five national research centres, four universities, four helicopter manufacturers and one SME) was created in the frame of an EU-project in order to create an experimental database for the validation of 3D-CFD and comprehensive aeromechanics methods for the prediction of unsteady viscous flows including rotor dynamics for complete helicopter configurations, i.e. main rotor – fuselage – tail rotor configurations with emphasis on viscous phenomena like flow separation and transition from laminar to turbulent flow. The wind tunnel experiments have been performed during two weeks in spring 2008 in the large low-speed facility of the German-Dutch wind tunnels (DNW-LLF) on a Mach-scaled model of a modern transport helicopter. The fuselage is based on a NH90 model (including all control surfaces). The configuration consists of an articulated four-bladed main rotor (R = 2·1m) with ONERA 7AD rectangular rotor blades (c = 0·14m) with parabolic and anhedral tip and a two-bladed tail rotor (R = 0·383m) with rectangular untwisted blades (c = 0·074m) based on a BO105 model. Trimming at the nominal speed of 956rpm was done to weight, propulsive force, lateral force and tail rotor thrust coefficients, while the main and tail rotor tip Mach numbers were kept constant. Clear boundary conditions were found to be of higher importance than wind tunnel-simulations as close as possible to free flight. Therefore, the 6m x 8m closed test section has been used. Velocity profiles have been measured at the inflow plane in order to define accurate boundary conditions in the CFD simulations by means of hot-wire anemometry and wall pressures by means of pressure taps at the wind-tunnel walls. The measurement comprised global forces of the main rotor and the fuselage, normal force and bending moment acting on the horisontal stabiliser, axial force and torque of the tail rotor, steady and unsteady pressures, transition positions, stream lines, position of flow separation, velocity fields in the model wake, around the model fuselage and on the upper surface of the advancing and retreating rotor blades, vortex trajectories and elastic deformations of the main and tail rotor blades. Furthermore the so called model-related parameters were measured for each test condition. The paper illustrates sample results of the more than 710 data points. A brief description of the available data is given in the data base description.

2.0 EXECUTED TEST MATRIX

The executed test matrix is summarised in Table 1: TC 1 represents measurements of the isolated fuselage over a wide range of shaft angles with rotating stubs on the hubs in order to get the fuselage polars as well as the hub tare loads for the following test cases:

TC 1.1 – polar for TC 2 (pitch-up)
TC 1.2— polar for TC 3 (cruise) and TC4 (tail shake)
TC 1.3 – polar for TC 5 (dynamic stall)
TC 1.4 – polar for TC 6 (high speed) [not performed, extrapolated]

At the nominal conditions (predicted by the Eurocopter HOST code) a sensitivity study was performed to evaluate the effect of different control settings (collective and cyclic) on the hub tare loads. TC 2 – TC 6 are with rotor blades on the hubs.

TC 2 (pitch-up): The correct shaft angle setting was identified during the test based on analysis of the dynamic content of the stabiliser leading edge dynamic pressure sensors as well on the dynamic content of the stabiliser balance. For this, a range of shaft angles was measured around the HOST prediction. Large vibrations were present at this low speed as expected in this configuration.

Table 1
Executed test matrix

TC	M_{WT}	M_{MR}	M_{TR}	μ
1.1	0·059	0·617	0·563	0·096
1.2	0·204	0·617	0·563	0·331
1.3	0·059	0·617	0·563	0·096
2	0·204	0·617	0·563	0·331
3 / 4	0·259	0·617	0·563	0·420
6	0·280	0·617	0·563	0·454

TC 3 (cruise): All parameters were pre-defined by the HOST prediction and performed as prescribed, with low vibration.

TC 4 (tail shake): The correct shaft angle setting was identified during the test based on analysis of the dynamic content of the fin leading edge dynamic pressure sensors as well on the dynamic content of the fuselage balance. For this, a range of shaft angles was measured around the HOST prediction, which was identical to TC 3. After investigation of data TC 3 was selected as condition for TC 4 as well.

TC 5 (dynamic stall): The HOST prediction delivered values that were very close to the maximum available power provided by the model. Since the condition was declared as critical, with high loads for all components of the model, the definition of the TC 5 case was kept open to the limits of the model experienced during the test. However, the wind tunnel and rotor tip speed Mach numbers were fixed, but allowance was given to modify the trim parameters. The goal was to come as close as possible to the high thrust level, while the shaft angle, propulsive force were free to be varied. Power, vibration, control and actuator force limits were reached. This case was then selected as the dynamic stall case, which showed a pitch link force spike in the third quarter of the revolution – an indicator for stall inception.

TC 6 (high speed): A high advancing blade tip Mach number of 0·91 was envisaged – here with reduced stall – thus an increased tip Mach number was chosen. Again, large dynamic loads and rotor power were expected. Therefore, as in TC 5, the actual trim settings were left open according to the limits encountered during testing. Power and control limits were reached. This was selected finally as the high-speed case, leading to a tip Mach number of the advancing blade of 0·897.

All pressure, SPR, PIV etc. measurements were then performed with continuous repeats of these conditions. It was found that a very good repeatability was present of the trim and balance data throughout the rest of the test.

3.0 FUSELAGE THERMOGRAPHY

The infrared technique is capable of delivering two-dimensional information of the boundary layer state in wind tunnels. As described in literature[6-8], remarkably large areas can be observed for the occurrence and location of transition lines. During the GOAHEAD test, DLR has been responsible for the detection of the laminar-turbulent transition on the fuselage of the model with infrared thermography. Two infrared cameras have been used for the infrared measurements: one for the side view and another one for the top view of the model fuselage. The cameras have been installed at an appropriate position near the tunnel wall behind devoted orifices in the tunnel wall. Since the DNW-LLF is an atmospheric wind tunnel no special infrared windows were required. The camera for the side view was equipped with a lens for a 10° x 7·5° field of view

https://doi.org/10.1017/S0001924000005492 Published online by Cambridge University Press

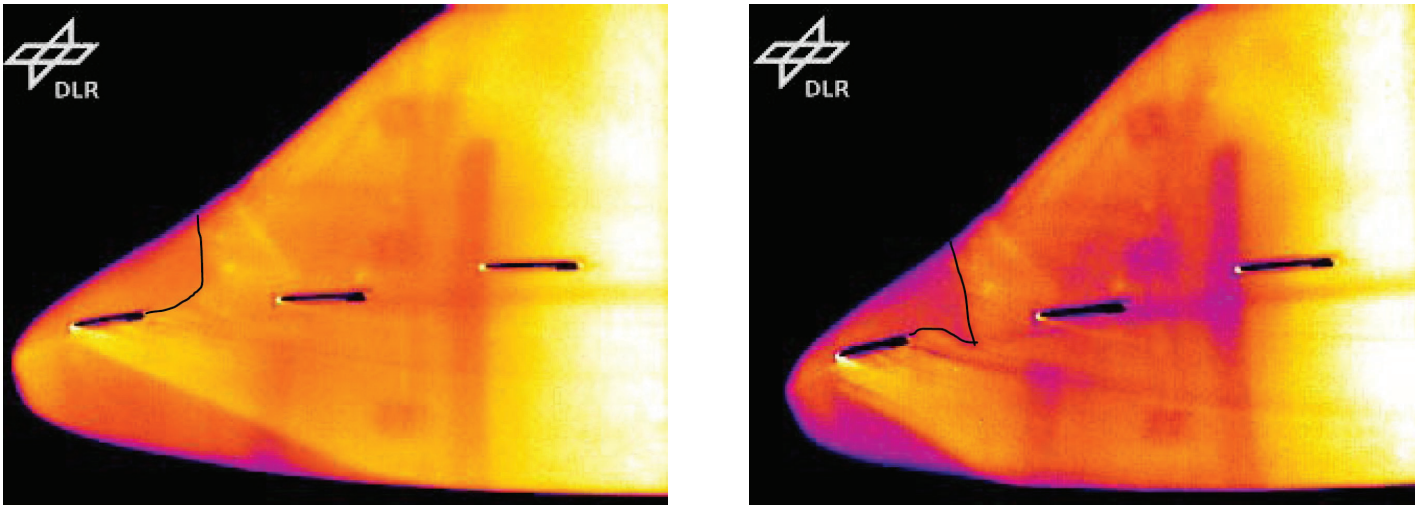

(a) (b)

Figure 1. (a) Infrared image of data point 185 (side view) of the front part of the fuselage at M_{WT} 0·259 and α_{fus} = –1°.
(b) Infrared image of data point 183 (side view) of the front part of the fuselage at M_{WT} 0·259 and α_{fus} = –5°.

and has been mounted on a special displacement unit, which allowed an adjustment of the view from the infrared computer via remote control and more than one measurement at a data point at different regions of the model. The camera for the top view was equipped with a lens for a 20° x 15° field of view and has been mounted on a tripod head allowing an exact adjustment of the upper region of interest.

The cameras used were FLIR System SC3000 cameras with a GaAs QWIP chip (Quantum Wall Infrared Photo detector), cooled down to 70K by liquid nitrogen and operated at 50 frames/s (with averaging), and characterised by a temperature resolution of 20mK. Since the GOAHEAD model fuselage had been constructed from Carbon fibre-reinforced polymer, no modification for the infrared measurements was necessary. A clear detection of the laminar-turbulent transition requires a small difference (some Kelvin) in the temperature of the model and the incoming flow in order to generate heat transfer. At high Mach numbers this temperature step could be achieved by warming up the model with the frictional heat of the flow and additionally switching the cooler of the wind tunnel for a short time off. Two special infrared radiators have been installed in the nose of the GOAHEAD model. The radiators, with a maximum power of 500W each, have been supplied with a regulated power supply. A small fraction of this power for only short periods of time was necessary for sufficient temperature steps in order to perform adequate infrared measurements. In the frame of the GOAHEAD wind tunnel test, infrared measurements have been performed during three days at 164 data points. A complete set of the results measurements has been placed in the data base. Some typical infrared images, sampled at different conditions, are shown and discussed in the following.

The infrared images of the side view for the dynamic stall measurements at M_{WT} = 0·259 are shown in Figs 1(a) and 1(b) for two different angles-of-attack. The laminar-turbulent transition (see the black lines as a guide to the eye) at this Mach number was further downstream and the first hot film acted like a tripping device producing turbulence in the nose region of the model.

The other installed camera for the top view has delivered additional information. Free transition could be found at the upper side of the nose at higher speeds (cruise speed and dynamic stall) and higher angles-of-attack (Fig. 2(a)). At low speed (pitch up) and lower angles of attack the transition is mainly forced by the pressure rise at the bend between the nose and the window and the bend in the side part (Fig. 2(b)). The free or forced transition at the side part of the fuselage could not be clearly detected due to the disturbances of the mounted hot films and especially their soldering points. As expected, the infrared heating inside the model lead to infrared images with higher contrast to detect the laminar-turbulent transition but also measurements without this heating lead to sufficient image quality.

4.0 INFLOW HOTWIRE MEASUREMENTS

For the aim of the GOAHEAD project it was necessary to qualify the test chamber inlet flow in order to ensure that the action of model rotors did not produce any sensible modification in the upstream flow. Additionally, numerical simulations needed this information in order to properly define the inflow conditions. The inlet flow field survey was carried out by means of a couple of triple hot wire directional probes[9-11] that have been successively positioned in a set of inlet points in order to measure the inflow velocity with and without the main and tail rotors. The probes have been previously calibrated, with respect to Reynolds number and velocity direction, in laboratory monitored conditions. The calibration procedure took into account the effects of temperature, pressure and humidity so that the calibration itself could be extended to the wind tunnel ambient conditions[12]. The test condition chosen for the inflow survey was the TC3 (cruise flight at Ma = 0·204). The probes were held by a double-prong sting (Fig. 3(a)) equipped with a two-component inclinometer in order to correct for possible bending during the test. As the strut was – on the whole – rather intrusive (Fig. 3(b)), its effect on the measurements was not negligible and the measured velocities were mainly regarded to the differences between the configurations with and without the rotors.

Actually, the measurement results did not show any evidence of significant rotors effects over the test chamber inflow. The measured differences in the speeds were less than 0·5% and the flow deflections in the order of one tenth of a degree or less. It has to be considered that these small values are comparable with the accuracy of the measurement technique[13]. Similarly, the action of the rotors

https://doi.org/10.1017/S0001924000005492 Published online by Cambridge University Press

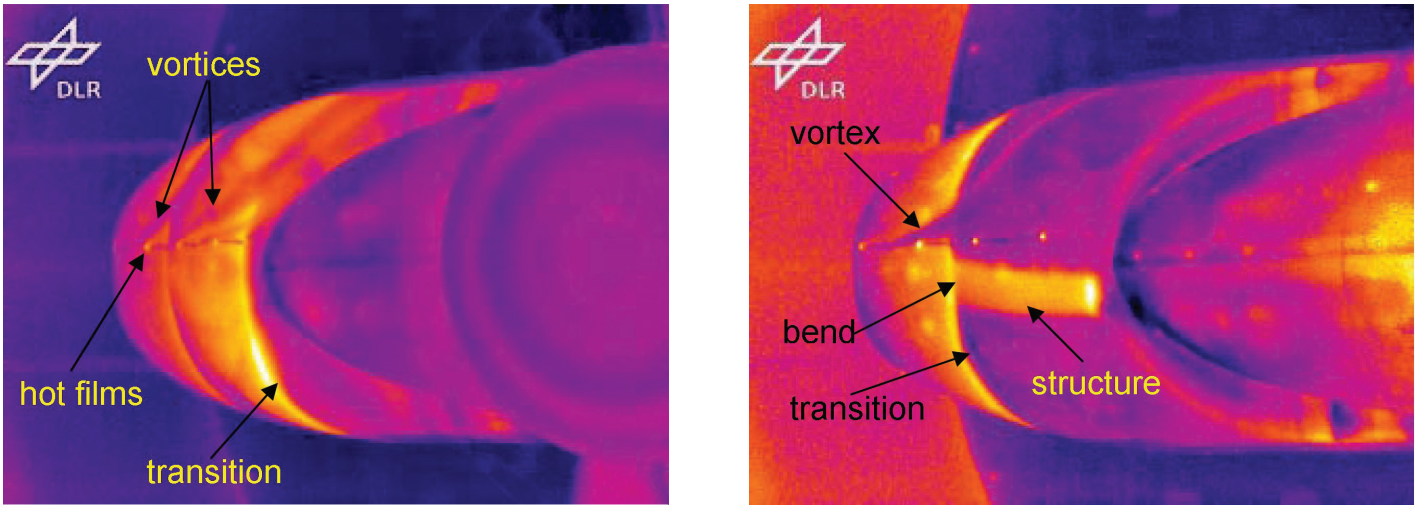

(a) (b)

Figure 2. (a) Infrared image of data point 147 (top view) of the front part of the fuselage at M_{WT} 0·204 and α_{fus} = –9°
(b) Infrared image of data point 131 (top view) of the front part of the fuselage at M_{WT} 0·059 and α_{fus} = 5°.

Table 2
Mean square values of the three velocity components measured in the inlet centre point in m^2s^{-2}

	$\overline{u'^2}$	$\overline{v'^2}$	$\overline{w'^2}$
Without rotors	0·003	0·014	0·025
With rotors	0·003	0·015	0·028

did not produce any important difference in terms of the turbulence levels. In both cases, with and without the rotors, the measured turbulence energy was in the order of $2*10^{-2}$ m^2s^{-2} which means that its value normalised by the square of the free-stream velocity was in the order of $4*10^{-6}$.

Due to the contraction effect[14] the turbulence was anisotropic with higher intensity in the cross-wise directions as can be seen from the Table 2 that presents the mean square values of the three velocity components measured in the inlet centre point (u is the stream-wise component, v is the component in the vertical direction and w is the span-wise component).

Figure 3(c) shows the comparison between the velocity spectra obtained, with and without the rotors, at inlet centre point: disturbances due to main and tail rotors are clearly recognisable but their contribution to the total turbulence energy is rather moderate as can be seen in Table 2: as mentioned before the order of magnitude of the turbulent energy does not change with the rotor action.

5.0 PRESSURE MEASUREMENTS

Steady and unsteady pressures have been measured on the fuselage by 292 pressure taps and 130 unsteady pressure transducers. The locations of the static pressure sensors (yellow dots), dynamic pressure sensors (red and blue dots) and hot films sensors (green dots) are indicated in Fig. 4. The steady pressure distribution on the fuselage for the fully equipped model in cruise/tail shake condition at M_{WT} = 0·204 is shown in Fig. 5.

Unsteady pressure data on fuselage have been recorded for the isolated fuselage model at three different Mach numbers (M_{WT} = 0·.059, 0·204 and 0·259), and the complete helicopter model at four Mach numbers (M_{WT} = 0·059, 0·204, 0·259 and 0·280). All unsteady pressures on the fuselage were gathered for 150 main rotor revolutions with 2,048 data samples per main rotor revolution, providing a main rotor azimuth resolution better than 0·176°. Figure 6 shows the comparison of the pressure time history for the cases of the isolated fuselage and the complete model at two different positions (wind shield and tail boom) at M_{WT} = 0·204. The pressure time history clearly indicates the effect of the main rotor on the fuselage pressure. Furthermore, the four blade passages and higher mean pressure values can be observed. For the isolated fuselage model, the four revolution periodicity has been also detected by the pressure. The wake shedding from the rotating hub equipped with the stubs can clearly be seen, but the signals showed considerably lower values (Fig. 6 sensor K14).

Additionally, 118 unsteady pressure sensors were installed on the main rotor, distributed on four rotor blades, including five sections on three rotor blades (spanwise at 97·5%, 91·5%, 82·5%, 70% and 50%), and 16 sensors were installed on blade 4 at the leading edge region (2% c upper and lower surfaces) in eight sections (95·25%, 90%, 87·5%, 85%, 80%, 75%, 60 % and 40%).

The unsteady pressure data on main rotor have been recorded at four different Mach numbers (M = 0·059, 0·204, 0·259, and 0·280) with the same sampling rate. Figure 7 shows the pressure distribution detected on the advancing blade (Ψ_{MR} = 90°) at spanwise position of 82·5% at M_{WT} =0·204. Although the cruise condition is still far from the maximum flight speed condition, the upper blade surface indicates an abrupt drop in the pressure distribution at about the 30% of the blade chord, indicating the presence of a shock wave.

6.0 BLADE HOTFILM MEASUREMENTS

In order to determine the boundary state on the blades, 40 hot film sensors were glued on four sections of blades 1 and 3 for the wind tunnel tests (Fig. 8). Hot film arrays from TAO Systems were implemented and conditioned with units specially designed and manufactured by ONERA and located into the main rotor for the tests.

The signals have been analysed for the tested configurations (TC2 to TC6) and an attempt was made to evaluate the boundary layer state in all the tested configurations, even if a majority of the data could not been used due to experimental difficulties. The analysis of hot film signals was done computing the mean and RMS values using a phase average method. In the cruise condition case (TC3-4), at M_{WT} = 0·204, a typical mean value signal (X/C = 14%) is plotted

https://doi.org/10.1017/S0001924000005492 Published online by Cambridge University Press

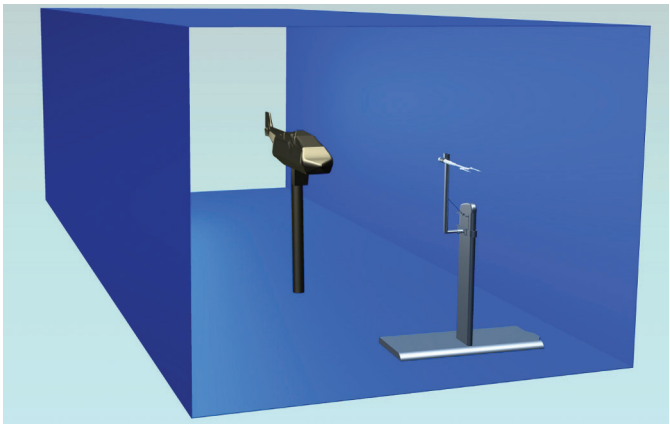

(a) General overview

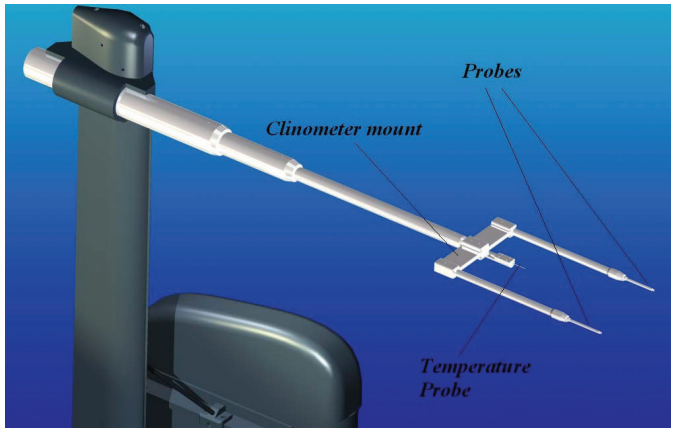

(b) Detail of the probe sting

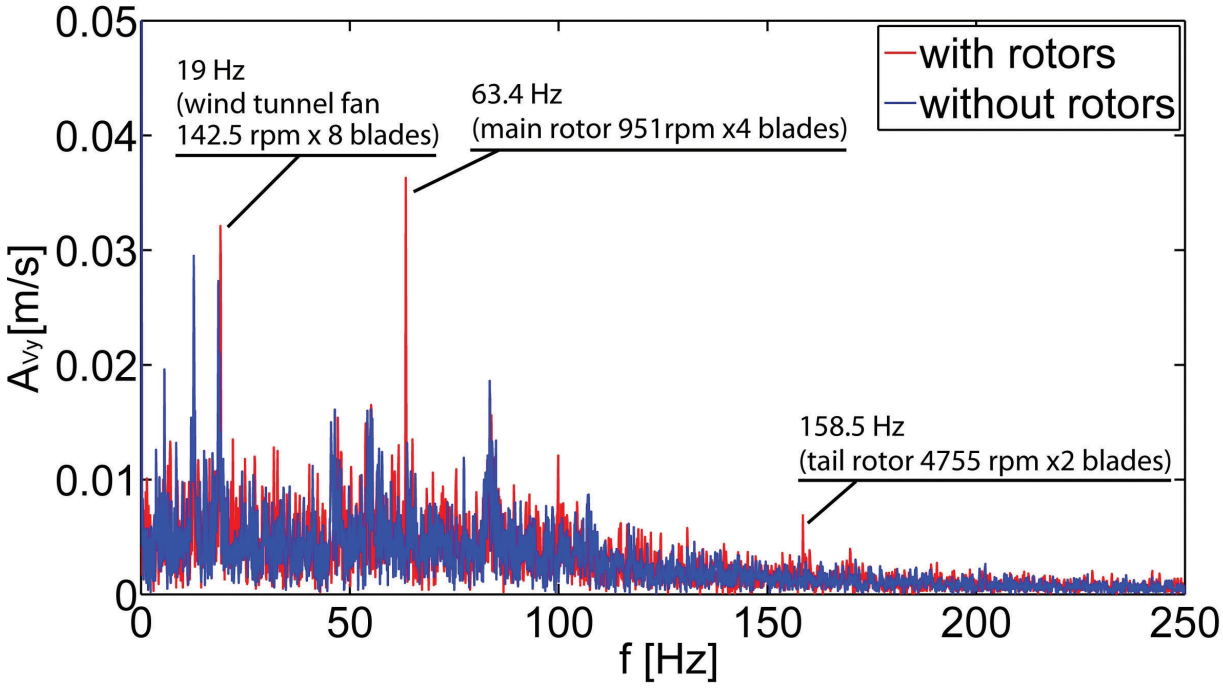

(c)

Figure 3 (a) and (b) Inflow measurement layout, (c) Measured in-flow velocity fluctuations over the frequency.

versus the rotor azimuth angle in Fig. 9: the abrupt increase of the level corresponds to a change from laminar to a turbulent state of the boundary layer, a sudden decrease illustrates a change from a turbulent to a laminar state[15]. The V_{mean} hot film signals plotted in Fig. 9 can be assimilated to the local boundary-layer friction coefficient evolution versus the azimuthal rotor angle. In turbulent condition the level is higher than in laminar state. Moreover, the RMS values exhibit peaks for each abrupt evolution of the mean level, which confirms the turbulent to laminar and laminar to turbulent passages[16,17]. From this analysis, a state of the boundary layer is proposed for this location (X/C = 14%) and two spanwise sections (Y/R = 60% blade 3 and 80 % blade 1) in Fig. 10. Along the rotor cycle, blue parts represent the laminar regions, red parts the turbulent ones; grey regions of the diagram are relative to separated zones. In the outer section (Y/R = 80%) the boundary layer is laminar with some perturbations at azimuth angles varying from 50° to 120° (white and blue regions). This boundary-layer state is found over the leading edge part of the blades (0% < X/C < 14%). Further downstream a monotonous evolution of the measured mean level indicating a turbulent state of the boundary layer.

7.0 FLOW VELOCITY FIELD MEASUREMENTS

PIV measurements have been performed as well on the isolated fuselage (see Fig. 11) as on the full helicopter model for different flight conditions by CIRA, DLR and DNW[18]. The flow region downstream the rotating hub and downstream the rear hatch of the helicopter model has been investigated for flight cruise condition (TC3-4). Three-component PIV measurements have been carried out

https://doi.org/10.1017/S0001924000005492 Published online by Cambridge University Press

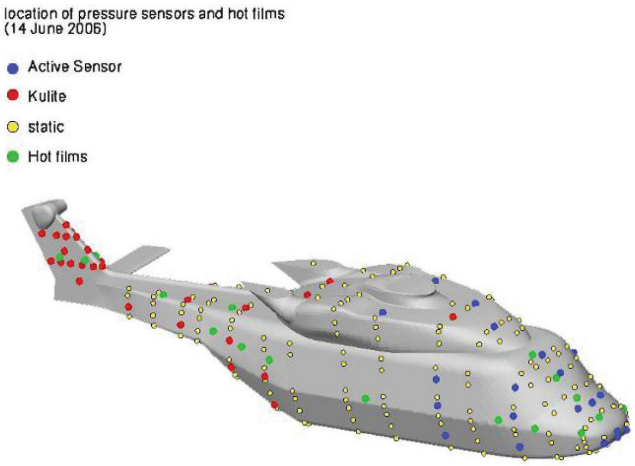

Figure 4. Sensor location on the fuselage model.

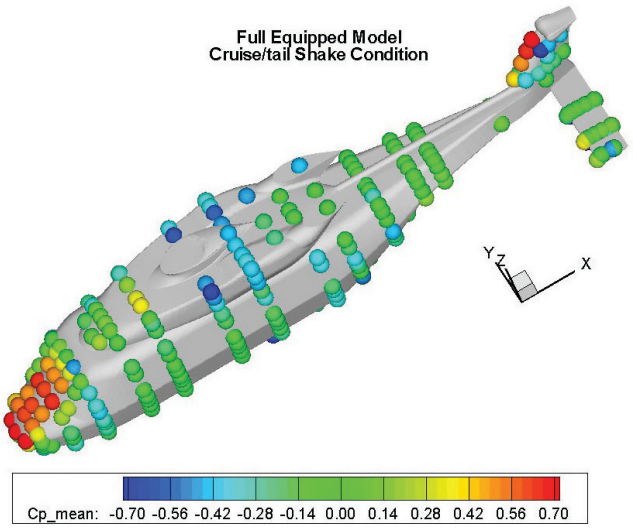

Figure 5. Mean pressure for fully equipped model.

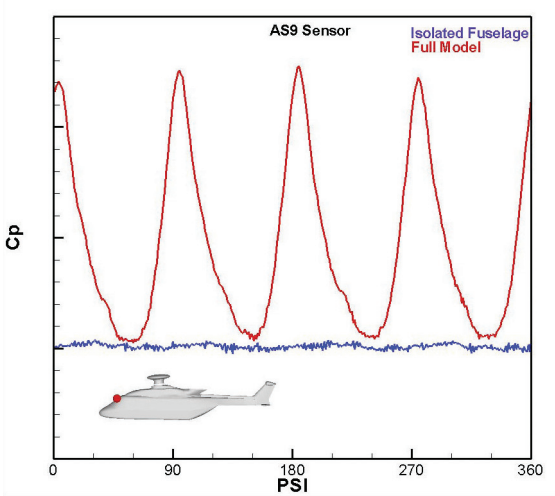

(a)

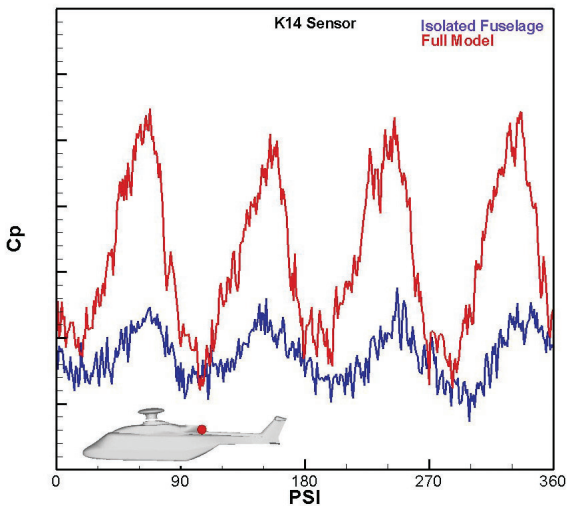

(b)

Figure 6. Isolated fuselage and complete model pressure time history comparison at M_{WT} = 0·204.

in phase with the main rotor azimuth angle on several cross planes downstream the rotating hub (Flow region PIV1). For each cross plane five different azimuth angle positions have been investigated (Ψ_{MR} = 0°, 22·5°, 45°, 67.5° and 90°).

The sample files presented in Figs 11 and 12 show the wake flow behind the rotating hub, for the cases of isolated fuselage (test condition TC1) and full model (test condition TC3-4). The pictures show the mean phase locked velocity field for the main rotor azimuth angle of 0°, the velocity magnitude is shown colour coded together with streamline computations.

Analogous for flight cruise condition, the flow field region downstream the rear hatch of the fuselage has been characterised by measuring the three velocity components on several cross planes (flow region PIV2) synchronising the measurement system with the rotor azimuth position of $\psi_{MR} = 0°$.

The Figs 13 and 14 clearly show two counter rotating vortices shedding by the lower region of the fuselage and their position moving downward.

The pitch up flow condition (test condition TC2) has been investigated measuring the flow field behaviour on a vertical longitudinal plane above the horisontal stabiliser (flow region PIV3). In Fig. 15 the orthogonal component of the vorticity is shown colour coded

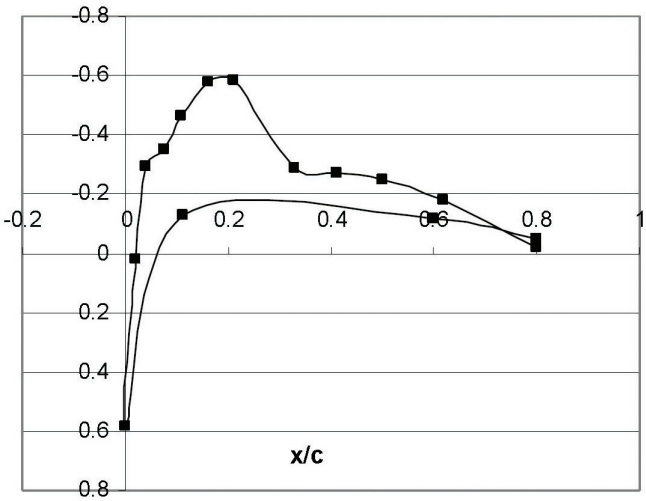

Figure 7. Blade rotor pressure distributions at 82·5% spanwise (MWT = 0·204, Ψ_{MR} = 90°) .

https://doi.org/10.1017/S0001924000005492 Published online by Cambridge University Press

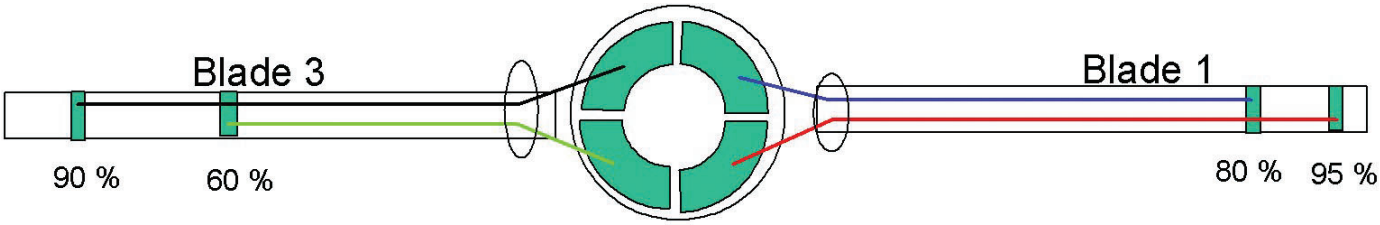

Figure 8. Installation of hot films on blades.

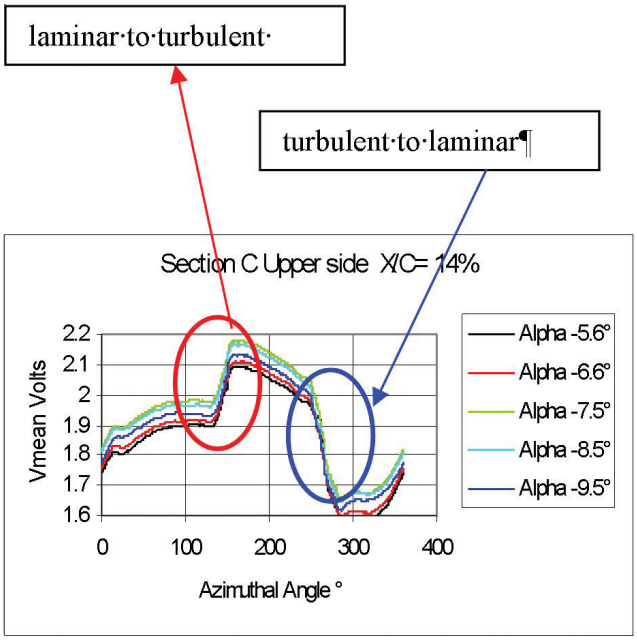

Figure 9. Hot Film signals evolution in a rotor cycle.

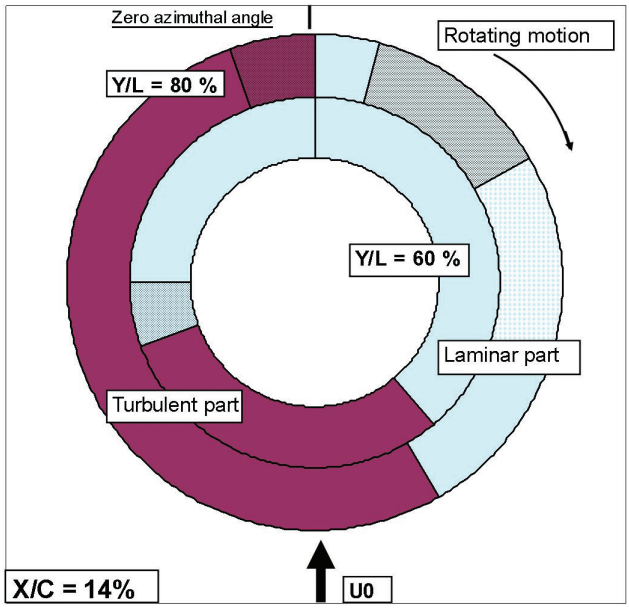

Figure 10. TC3-4 boundary layer state at *X*/*C* = 14%.

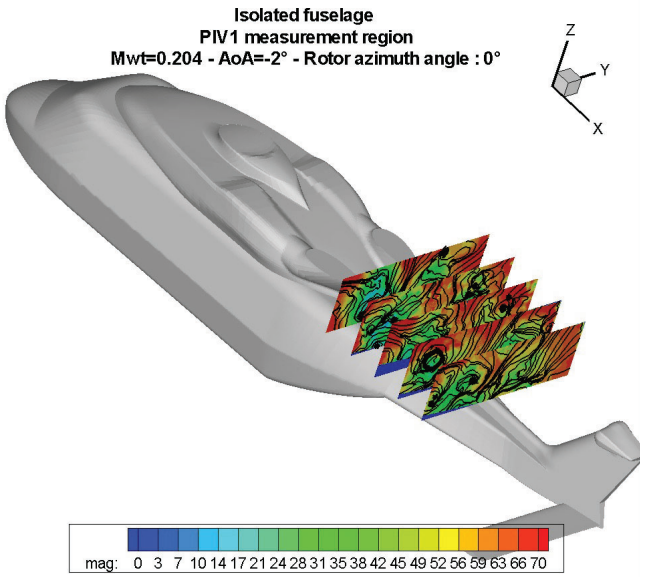

Figure 11. TC1 – PIV1 - Isolated fuselage Ψ_{MR} = 0°.

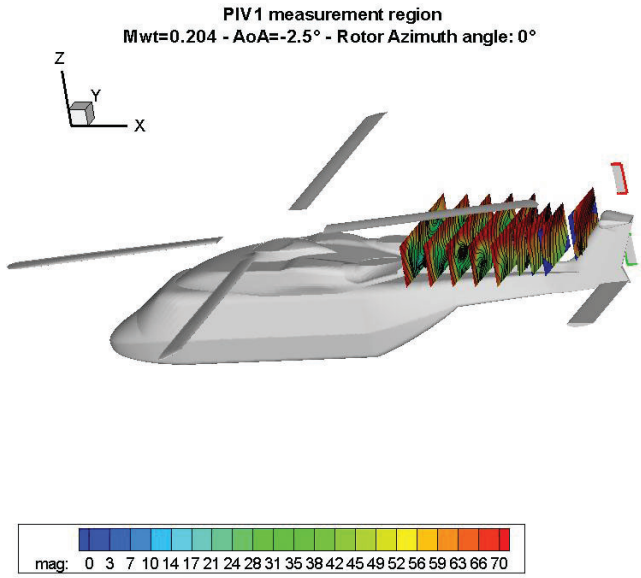

Figure 12. TC3-4 –PIV1 -Full model for Ψ_{MR} = 0°.

https://doi.org/10.1017/S0001924000005492 Published online by Cambridge University Press

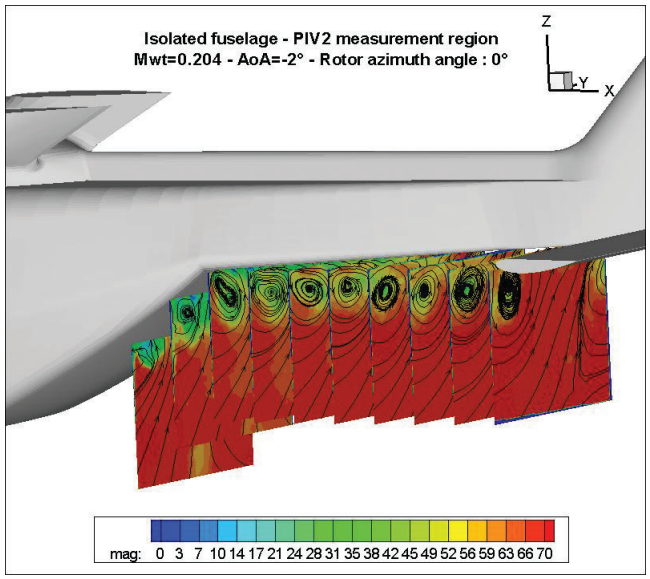

Figure 13. TC1 – PIV2 isolated fuselage for Ψ_{MR} = 0°.

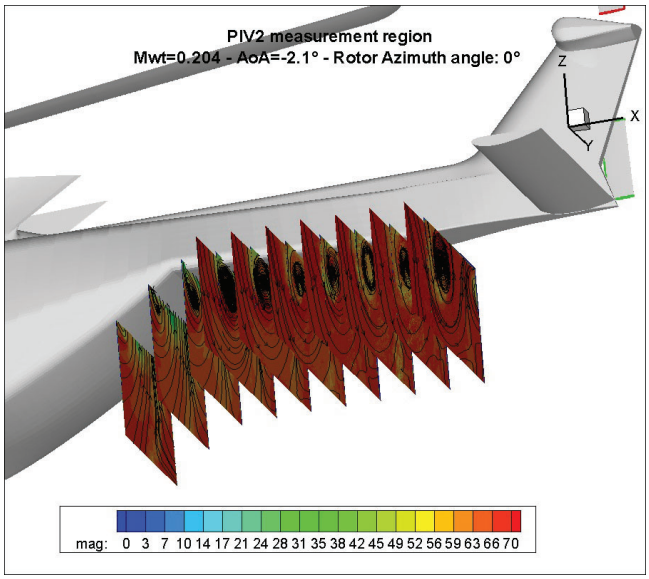

Figure 14. TC3-4 - PIV2 Full model for Ψ_{MR} = 0°.

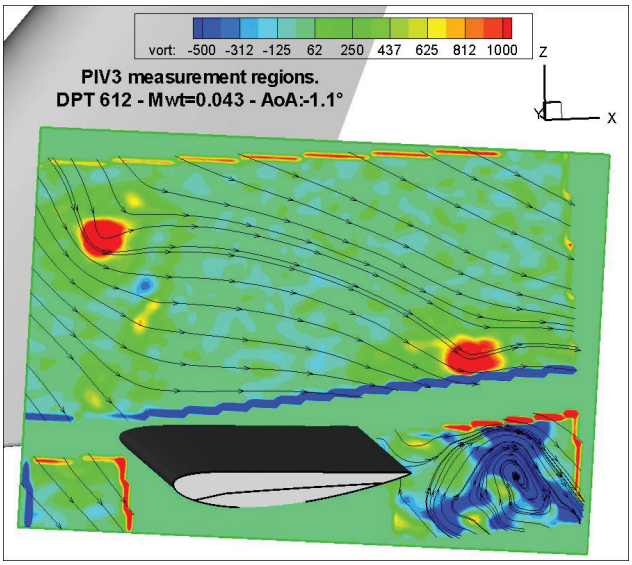

Figure 15. TC2 – PIV3 full model Ψ_{MR} = 142·6°.

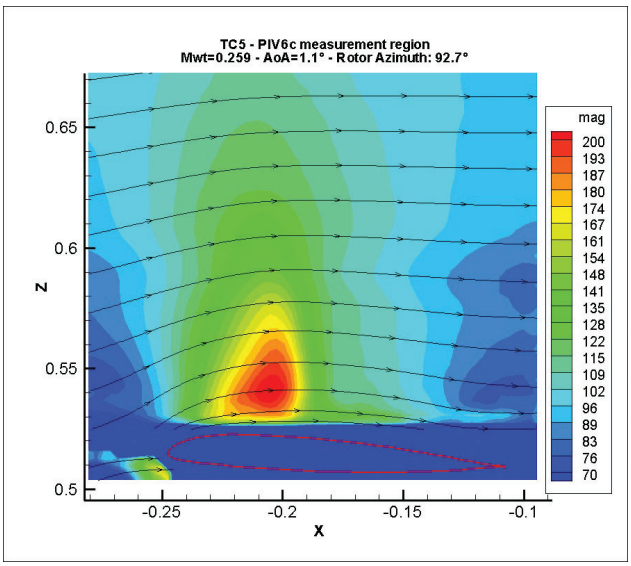

Figure 16. Advancing blade Ψ_{MR} = 90°.

together with streamline computations. Two vortices coming from the tip rotor blades are clearly visible above the horisontal tail plane and a strong circulation region due to flow separation is detected downstream the stabiliser.

In addition to the larger observation areas in the near and far wake of the helicopter model two close up recording areas in the proximity of the rotating main rotor blades where chosen: The tip region of the advancing blade (shown in Fig. 16), a flow field with embedded shock waves, and the flow field above the retreating blade at high flight velocities characterised by dynamic stall (Fig. 17).

8.0 BLADE DEFLECTION MEASUREMENTS

The rotor blade deflections were measured by means of SPR (stereo pattern recognition). The SPR technique is based on a three-dimensional reconstruction of visible marker locations by using stereo camera images[19]. Output of the SPR measurements are spatial positions of markers painted on the upper surface of all of the four rotor blades and on top of the rotor hub fairing.

Four SPR cameras were mounted above the model outside the ceiling of the wind-tunnel test section with a fixed orientation to each other. They were located in front and in the back, to the left and to the right of the model, with focus on the advancing and the retreating side of the rotor disk such that almost the entire disk could be observed by all cameras. A total of 28 markers with a diameter of 25mm were painted on the upper side of each rotor blade – 14 at the leading and 14 at the trailing edge covering the blade from 19% to 96% radius – in compliance with distance requirements to hot film sensors and dynamic pressure sensors, see Fig. 18).

Measurements were done with azimuth increments of 11·25 deg, respectively 32 azimuth positions per revolution such that the analysis allows to synthesise the lower harmonics from 0-5/rev from the time history of the blade motion with good confidence, the 6/rev

https://doi.org/10.1017/S0001924000005492 Published online by Cambridge University Press

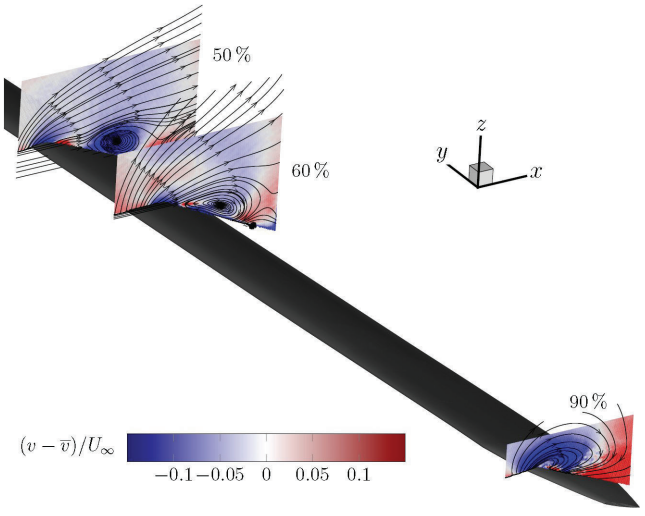

Figure 17. Dynamic stall PIV measurement results at the retreating blade Ψ_{MR} = 270°.

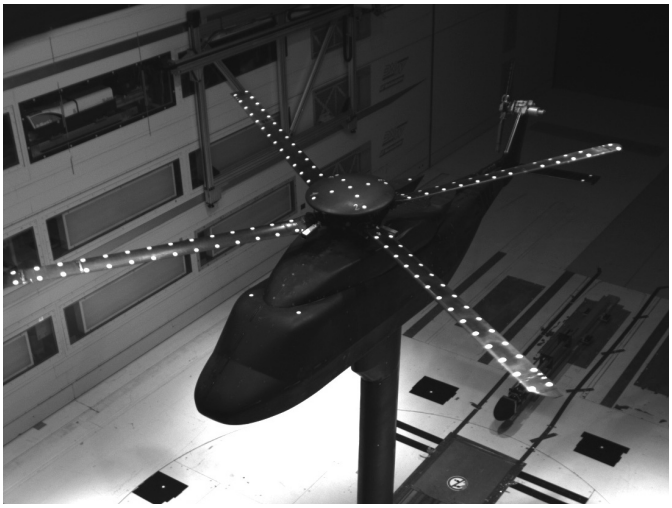

Figure 18. View from SPR camera front left.

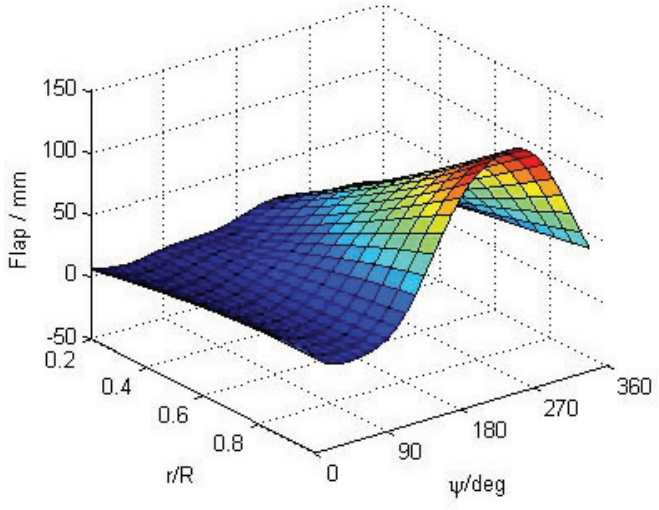

Figure 19. Blade flap motion of TC2 blade #1.

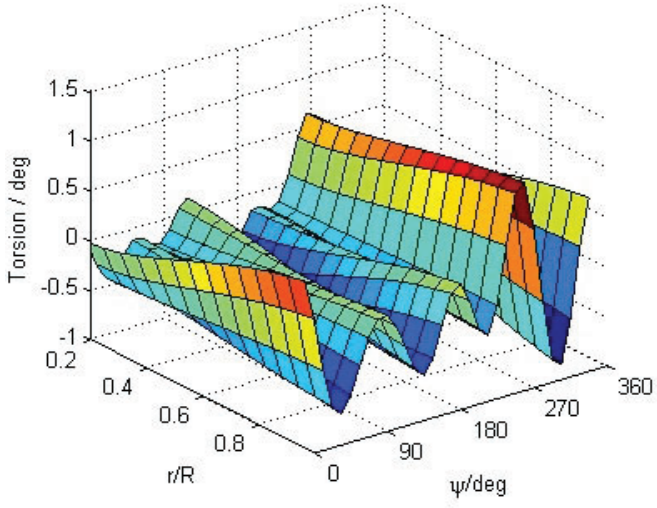

Figure 20. Blade elastic torsion motion of TC2 blade #1.

with reduced confidence, and the 7 and 8/rev with low confidence. On every azimuth position 30 images were taken for averaging purposes in order to get smooth data with reduced errors and eliminated non-harmonic vibrations.

In the post-processing all SPR marker co-ordinates in wind-tunnel system were transformed into the rotor hub system to analyse the blade motion parameters in flap, lead-lag, and torsion[20]. The flap and lead-lag motion can be extracted from the distance between the radial position of the quarter chord line and a straight line defined by the current azimuth position of the blade. The pure elastic pitch deformation can be calculated by the distance of the *s*-co-ordinate of the front and rear blade markers, the associated pitch control angle, the pre-twist angle and the pitch offset in *s*-direction due to the different distance of the front and rear blade markers to the quarter chord line. Here the accuracy is depending on the chord-wise distance of the SPR markers (96mm) and the SPR recognition accuracy (0·4mm), which leads to ±0·24 deg.

Since the SPR technique is based on discrete azimuth steps and a limited number of those radii where SPR markers were placed, an approach with Fourier series and mode shape coefficients was used to allow for an analytical synthesis of continuous data in both radial co-ordinate and azimuth that are smooth even in second or higher derivatives. The representation is based on a best fit of the lower blade mode shapes along radius and on a Fourier series in azimuth direction. As a result all blade motions are analytically described in both radial co-ordinate and azimuth, such there is no limitation on discrete azimuth steps. Samples for blade flap and elastic torsion are shown in Figs 19 and 20).

9.0 DATABASE

The GOAHEAD data base contains the measured data in terms of wind tunnel conditions, model parameters, model pressure distributions, main rotor blade deformation, boundary-layer measurements and flow-field velocity measurements for all the test conditions.

The wind-tunnel condition data consist of wind tunnel velocity, static and dynamic pressure, density, temperature, Mach number, etc. Furthermore the inflow velocity and turbulence profile up stream the model were stored together with the static pressure distribution on the test section walls.

The model parameters contain all measurement carried out directly on the model/rotor rig except for pressure, hot films and blade deformation. The following quantities are stored for each data point:

https://doi.org/10.1017/S0001924000005492 Published online by Cambridge University Press

- the fuselage angle of attack and side slip angle;
- the static and dynamic loads on main rotor, fuselage and horisontal tail plane;
- the main rotor speed, power, torque; the main rotor control angle (pitch, flap and lead-lag), and the pitch link loads;
- the tail rotor speed, thrust and torque and control angles (pitch and flap);
- the blade bending, lead-lag and torsion moments.

The data are available as time history or as Fourier coefficients. The pressure data contains the steady pressure data on the fuselage and the unsteady pressure data on the fuselage, main rotor and tail rotor.

The blade deformation contains the data obtained by the strain pattern analysis (SPA) technique and by the stereo pattern recognition (SPR) technique. The SPA provided the bending, lead-lag and torsion elastic deformation whereas the SPR provided the full blade displacement coupling the blade movement and the blade deformation.

The boundary-layer folder contains all measurements data related to the state of the boundary layer on both fuselage and main rotor. The hot film data on fuselage and main rotor, the micro tuft movies recorded by the surveillance cameras, and the images recorded by the infrared cameras are stored.

The flow-field velocity contains the results of the PIV measurements on the different regions around the model for the different test cases. Together with the three components velocity fields the post processing data are stored.

10.0 CONCLUSION

The flow field in the vicinity of a fully equipped helicopter rotor model has been investigated by means of unsteady and steady pressure transducers, infrared imaging, hot wire and hot film anemometry and particle image velocimetry. The results have been used in order to fill a meaningful database for helicopter CFD code validation. Although, the large-scale application of optical testing methods and the traversing of laser and camera equipment was hampered by the closed wind tunnel test section a quite complete set of PIV data could be sampled and is now ready to be used. The infrared thermography was cost efficient since it did not require any wind tunnel occupation time and delivered valuable results. The sampling of steady and unsteady pressure data work well, but a more complete online monitoring of the data had helped to make decisions during the test. The hot wire probes measured the turbulence levels at the test section entrance at rotor-on and rotor-off conditions reliably, but the hot films attached to the main rotor blades and the fuselage failed in some cases. The blade deformation measurement by the optical SPR technique delivered quite a complete set of data for all rotor test conditions.

ACKNOWLEDGEMENTS

The authors very much appreciate the co-operation with all participating partners, the EU and the wind-tunnel staff of DNW-LLF.

REFERENCES

1. HEINECK, J.T., YAMAUCHI, G.K., WOODCOCK, A.J. and LOURENCO, L. Application of three-component PIV to a hovering rotor wake, 2000. 56th annual forum of the American helicopter society, Virginia Beach, VA, USA.
2. MARTIN, P.B. and LEISHMANN, G.J. Trailing vortex measurements in the wake of a hovering rotor blade with various tip shapes, 2002. 58th annual forum of the American helicopter society, Montreal, Canada.
3. RAFFEL, M., SEELHORST, U. and WILLERT, C. Vortical flow structures at a helicopter rotor model measured by LDV and PIV, *Aeronaut J*, 1998, **102**, (1012), pp 221-227.
4. MURASHIGE, A., KOBIKI, N., TSUCHIHASHI, A., NAKAMURA, H., INAGAKI, K. and YAMAKAWA, E. ATIC Aeroacoustic Model Rotor Test at DNW, 2000, 24th European rotorcraft forum, Marseille, France.
5. VAN DER WALL, B.G. and RICHARD, H. Analysis methodology for 3C-PIV data of rotary wing vortices, *Experiments in Fluids*, 2006, **40**, pp 798-812.
6. FEY, U., DE GROOT, K. and LE SANT, Y. Thermography as a tool in wind tunnel testing, 2004, European Wind Tunnel Association (EWA), ANE3-CT-2004-502889, Network of Excellence, Priority 4, Aeronautics and space, Deliverable 2/10/2004.
7. LE SANT, Y., MARCHAND, M., MILLAN, P. and FONTAINE, J. An overview of infrared thermography techniques used in large wind tunnels, *Aerospace, Sci and Tech*, 2002, **6**, pp 355-366.
8. QUAST, A. Detection of transition by infrared image technique, 1987, IEEE publication CH2449-7/87, ICIASF.
9. JORGENSEN, F.E. Directional sensitivity of wire and fibre film probes, *DISA Info*, 1971, **11**, pp 31-37.
10. CHEW, Y.T. and HA, S.M. The directional sensitivities of crossed and triple hot-wire probes, *J Phys E Sci Instrum*, 1988, **21**, pp 613-620.
11. LEKAKIS, I.C. ADRIAN, R.J. and JONES, B.G. Measurement of velocity vector with orthogonal and non-orthogonal triple-sensor probes, *Exp Fluids*, 1989, **8**, pp 228-240.
12. DURST, F., NOPPENBERGER, S., STILL, M. and VENZKE, H. Influence of humidity on hot-wire measurements, *Meas Sci Technol*, 1996, **7**, pp 1517-1528.
13. MACIEL, Y. and GLEYZES, C. Survey of multi-wire probe data processing techniques and efficient processing of four-wire probe velocity measurements in turbulent flows, *Experiments in Fluids*, 2000, **29**, pp 66-78.
14. HAN, Y.O., GEORGE, W.K. and HJARNE, J. Effect of a contraction on turbulence. Part 1: Experiment, 2005, AIAA 2005-1119.
15. SÉMÉZIS, Y. and BEAUMIER, PH Determination de l'état de la couche limite sur des sections de pale d'helicoptère al'aide de films chauds, 1995, 31ème colloque 3AF, 27-29 March 1995, Paris, France.
16. SÉRAUDIE, A., PERRAUD, J. and MOENS, F. Transition measurement and analysis on a swept wing in high lift configuration, 2002, 23rd Congress of ICAS Toronto, 8-13 September 2002, Canada.
17. PERRAUD, J., SÉRAUDIE, A. and MOENS, F. Transition on a high-lift swept wing in the European project EUROLIFT, *J Aircr*, September-October 2004, **41**, (5).
18. DE GREGORIO, F., PENGEL, K. and KINDLER, K. Industrial measurement campaign on fully equipped helicopter model, 2010, 15th Int Symposium on Applications of Laser Techniques to Fluid Mechanics, 7-10 July 2010, Lisbon, Portugal.
19. PENGEL, K., MÜLLER, R. and VAN DER WALL, B.G. Stereo pattern recognition – the technique for reliable rotor blade deformation and twist measurements, 2002, AHS International Meeting on Advanced Rotorcraft Technology and Life Saving Activities, Utsunomiya, Tochigi, Japan.
20. SCHNEIDER, O. Analysis of SPR measurements from HART II, *Aerospace Sci and Tech*, 2005, **9**, (5), pp 409-420. Elsevier.
21. DE GROOT, K. Application of the infrared technology for investigations of the boundary layer, 2005, ONERA/DLR meeting MOTAR, Lille, France.
22. SCHNEIDER, O., VAN DER WALL, B.G. and PENGEL, K. HART II blade motion measured by stereo pattern recognition (SPR), 2003, 59th Annual Forum of the American Helicopter Society, Phoenix, USA.
23. SCHNEIDER, O. and VAN DER WALL, B.G. Final analysis of HART II blade deflection measurement, 2003, 29th European Rotorcraft Forum, Friedrichshafen, Germany.